Title

Maximum likelihood analysis for the Cabibbo-Kobayashi-Maskawa matrix

Journal

Physical Review D, 49(3)

ISSN

2470-0010

Authors

Choong, Woon-Seng

Silverman, Dennis

Publication Date

1994-02-01

DOI

10.1103/physrevd.49.1649

Maximum likelihood analysis for the Cabibbo-Kobayashi-Maskawa matrix

Woon-Seng Choong and Dennis Silverman
Department of Physics, University of California, Irvine, Irvine, California 92717
(Received 10 August 1992; revised manuscript received 29 March 1993)

The probability of possible values for the four angles of the CKM matrix are determined by finding the χ^2 values for each choice of angles fitting to ten standard experiments. The χ^2 isosurface plots are first displayed in the space of three of the CKM angles showing the dependence of the bounds on δ and greatly improving the lower bound on V_{cb}. The maximum likelihood χ^2 contour plot in the ρ-η plane shows the probability of each location for the vertex of the unitarity triangle which controls CP-violating asymmetries in B^0 decays. We find for $m_t = 150$ GeV that at the 2σ level the signal for asymmetries measuring $\sin(2\beta)$ is at least $\sin(2\beta) \geq 0.25$. At the 1σ level the signal is at least $\sin(2\beta) \geq 0.40$, with the preferred range of $\sin(2\beta) = 0.6 \pm 0.2$.

PACS number(s): 12.15.Hh, 11.30.Er, 12.15.Mm, 13.20.He

I. INTRODUCTION

The analysis of experimental constraints on the four Cabibbo-Kobayashi-Maskawa [1,2] (CKM) angles is rather standardized [3,4]. It involves showing the 1σ contours in two parameters (ρ, η) for each experiment separately, for a specific choice of the third and fourth CKM parameters. In this work, however, all of the standard ten experiments are combined to form a joint χ^2 and evaluated for all values of the four CKM angles. Contours for the χ^2 which correspond to the equivalent confidence levels (C.L.'s) for 1σ, 2σ, and 3σ are then found in the parameter space of the four angles. The displays of fixed χ^2 surfaces in three angular dimensions for given choices of θ_{12} ($\simeq \lambda$) show at once the dependence of the limits of the two smaller angles θ_{23} and θ_{12} on each other and on δ.

We also construct the ρ-η plot or the unitarity triangle using the maximum likelihood statistical method. The usual way the CKM parameters are analyzed is to assume central values of $s_{12}(\lambda)$ and V_{cb} or A in order to make the ρ-η plot. The maximum likelihood χ^2 method used here, however, takes each point in the ρ-η plot and then for these possible physical values of ρ and η searches all values of the CKM angles to find the smallest χ^2 which predicts this ρ and η and assigns this χ^2 to the point.

One conclusion from the maximum likelihood ρ-η plot is that even at the 2σ contours there is still a signal for the B factory at $\sin(2\beta) \gtrsim 0.25$, and at 1σ $\sin(2\beta) \geq 0.40$, with $\sin(2\beta) = 0.60$ the most likely value. We also show on these plots the regions which give good and poor values for each of the CP-violating B decay asymmetry experimental angles.

In Sec. II we give the values which we use for experimental results to constrain the CKM matrix elements. In Sec. III we present fixed χ^2 surfaces in three parameter projections from the four-dimensional CKM angle parameter space. In Sec. IV we present the maximum likelihood ρ-η plots.

II. EXPERIMENTS TO CONSTRAIN THE CKM MATRIX

We refer the reader to the review by Gilman and Nir [3] (GN) for descriptions of the experiments, detailed formulas for most of the experiments, references, and the form of the CKM matrix [5]. For the matrix elements of the mixing of the first two families, we use the GN values [3]: $|V_{ud}| = 0.9744 \pm 0.0010$, $|V_{us}| = 0.2205 \pm 0.0018$, $|V_{cd}| = 0.204 \pm 0.017$, and $|V_{cs}| = 1.02 \pm 0.18$. For the b quark matrix elements, we use the heavy quark symmetry result [6,7] on the exclusive $\bar{B} \to D^* \ell \bar{\nu}_\ell$ rate to give (although inclusive results are slightly higher [8,10,11])

$$|V_{cb}| = 0.037 \pm 0.006 \tag{1}$$

which includes the new B lifetime, $\tau_B = 1.5 \pm 0.16$ ps [9].

For V_{ub} we use the new results [10] from CLEO II for $|V_{ub}/V_{cb}|$ from the inclusive semileptonic decays of B mesons detecting b $\to$ u transitions. These are model dependent [10,11] with values from Altarelli *et al.* (ACCMM) [12] (0.075 ± 0.007), Koerner and Schuler (KS) [13] (0.055 ± 0.005), Wirbel, Stech, and Bauer (WSB) [14] (0.072 ± 0.007), and Isgur, Scora, Grinstein, and Wise (ISGW) [15] (with $\kappa = 1.00$) (0.082 ± 0.009). This leads to the weighted mean with a small standard error $|V_{ub}/V_{cb}| = 0.068 \pm 0.0033$. Upper bounds from exclusive B decay processes [16] from CLEO II of 0.08 to 0.13 at 90% C.L. are consistent with this. The above weighted mean has, however, $\chi^2 = 10.5$ for 3 degrees of freedom giving a low confidence level. Since this is really only one experiment with four theoretical models, the standard Gaussian approach is not really valid. A better approach may be to ignore the errors on each model, use the mean value of the models, and take the larger spread of values from the models as the true range that could contain the physical result. To be conservative and use the largest justifiable error, we fit a Gaussian about this mean with its σ set so that the resulting χ^2 is at the 50% C.L. For 3 degrees of freedom this is at $\chi^2 = 2.4$. (The 50% C.L. is the same as that where $\chi^2 =$ number of degrees of freedom for large N.) We then take

$$|V_{ub}/V_{cb}| = 0.071 \pm 0.013 \tag{2}$$

for use in χ^2. In this experiment, the 3σ contours are only to indicate the rough relative location with respect to the 1σ and 2σ contours.

B-$\bar{B}$ mixing gives a limit on $|V_{td}/V_{cb}|$ through x_d as

given in GN [3]. We use the values from GN except for the theoretical quantities we assume the results of lattice gauge calculations to be correct and use the recent lattice determination [17] $\sqrt{B_B}f_B = 220 \pm 40$ MeV which is larger but with about the same error as the GN [3] value of 150 ± 50 MeV. We also use the recent next-to-leading order QCD correction [18] $\eta = 0.55$, which is significantly different from the leading order correction $\eta = 0.85$. It is necessary to use the new value since the product $(B_B\eta)$ is QCD renormalization point invariant [19]. We use the range with errors rather than separate figures for separate values since the range is now only 20% and its effects are included in expanding the contours in the maximum likelihood method.

The ϵ parameter in the K meson system is the only direct evidence for CP-violation or for a nonzero value of η. We use the same values as GN with the exception of interpreting the range $1/3 < B_K < 1$ as 90% C.L. limits, so that at 1σ we take $0.47 < B_K < 0.87$, which is consistent with the range of lattice values [20] where the range runs from 0.48 to 0.90 at 1σ in the second reference.

The ninth and tenth experimental bounds are from the second-order weak short-distance contributions to the $K_L \to \mu\mu$ decay rate [4]. From this reference we take the largely uncertain but small off-shell two photon contribution (namely, between [4] 0.04×10^{-9} to 0.20×10^{-9}) to be zero to get the most conservative limit. This contribution is small compared to the combined errors in any case. Minimizing the χ^2 terms for both the new results of BNL [21] $[(6.86 \pm 0.37) \times 10^{-9}]$ and of KEK [22] $[(7.9 \pm 0.7) \times 10^{-9}]$ and subtracting the two photon unitarity [23] value $[(6.83 \pm 0.28) \times 10^{-9}]$, we find the bound on the short-distance contribution $B(K_L \to \mu\bar{\mu})_{SD} \leq (0.26 \pm 0.43) \times 10^{-9}$. The χ^2 after minimizing is 1.7, which must also be added to the total χ^2. For the equation controlling the short-distance effects see Refs. [24,25,4]. This puts an upper bound on $(1-\rho)^2$. The bound is most effective at high m_t.

Our maximum likelihood analysis mainly differs from a recently published one [26] in that we use the newly available results of the $K_L \to \mu\mu$, we use the new smaller CLEO II values for $|V_{ub}/V_{cb}|$, and we use the new lattice and QCD calculations on $\sqrt{B_B\eta}f_B$, which no longer necessitates treating it as a discrete parameter. It differs from others [27] who only analyze two experiments, $|\epsilon|$ and B_d-$\bar{B}_d$ mixing, in two variables, ρ and η.

III. RESULTS OF THE COMBINED PROBABILITY ANALYSIS

We computed the χ^2 from fitting all of the ten experimental constraints for all relevant values of the four angles of the CKM matrix.

In Fig. 1 are shown views of the three-dimensional χ^2 isosurfaces in θ_{13}, θ_{23}, and δ, with θ_{12} fixed at its

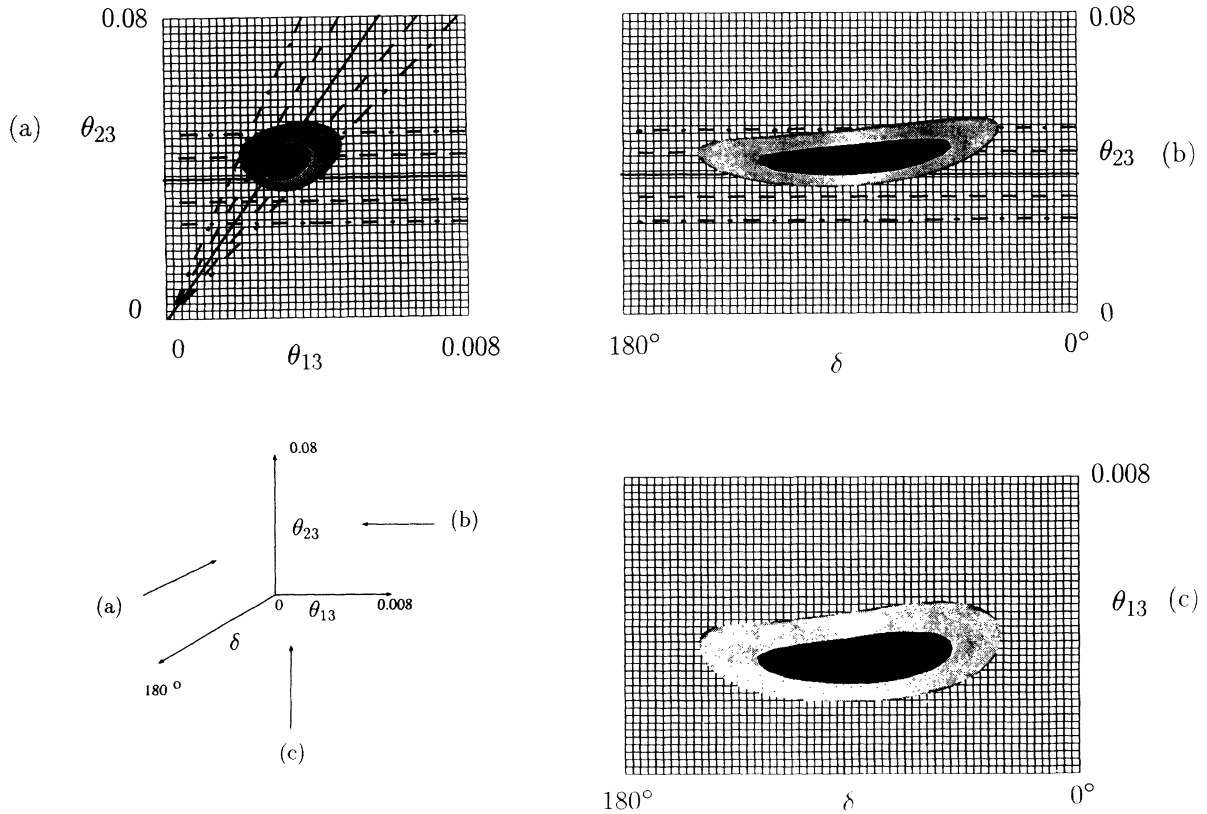

FIG. 1. Views of the three-dimensional angular plot showing the surfaces of $\chi^2 = 7.0$ and $\chi^2 = 12.8$ corresponding to 1σ and 2σ, respectively, with variables from $0 \leq \theta_{23} \leq 0.08$, $0 \leq \delta \leq 180°$, and $0 \leq \theta_{13} \leq 0.008$, for fixed $\theta_{12} = 0.223$ and $m_t = 150$ GeV. For comparison are shown in (a) and (b) central values and limits from Eqs. (1) and (2) without the maximum likelihood method. Central values are solid lines, 1σ limits are dashed lines and 2σ limits are dot-dashed lines.

most likely value of 0.223. The plot is for $m_t = 150$ GeV. The black inner surface is at $\chi^2 = 7.0$ and the outer surface is at $\chi^2 = 12.8$, corresponding to 1σ and 2σ confidence levels, respectively, for ten experiments with four parameters giving 6 degrees of freedom. We note the large range of δ that exists at 2σ, and that the cross sections of the surfaces in the (θ_{13}-θ_{23}) planes depend on δ, having less area at the extremes of δ. The central value for $s_{23} \simeq V_{cb}$ (solid line), and its 1σ (dashed lines) and 2σ (dot-dashed lines) error limits from Eq. (1) alone are plotted as horizontal lines in Figs. 1(a) and 1(b). Also plotted in Fig. 1(a), as slanted lines, are the central value for the ratio $s_{13}/s_{23} \simeq |V_{ub}/V_{cb}|$ (solid line) and its 1σ (dashed lines) and 2σ (dot-dashed lines) limits, from Eq. (2) alone. We note that the combined analysis 2σ isosurface only reaches down to the 1σ lower limit on $|V_{cb}|$ from Eq. (1) when taken alone. This great improvement on the lower limit on $|V_{cb}|$ results from the combined probability analysis.

IV. MAXIMUM LIKELIHOOD PLOT FOR VALUES OF ρ AND η

The real and imaginary parts of V_{ub} are typically shown in the $\rho - \eta$ plot, where ρ and η are the real and negative imaginary parts of V_{ub} after scaling out $A\lambda^3$ in the Wolfenstein parametrization [28] which is $V_{ub} = \lambda^3 A(\rho - i\eta)$, $V_{cb} = \lambda^2 A$, and $V_{td} = \lambda^3 A(1 - \rho - i\eta)$. From the angular parametrization the relation is

$$\rho + i\eta = V_{ub}^*/(|V_{cd}V_{cb}|) \approx s_{13}e^{i\delta}/(s_{12}s_{23}c_{13}) \ . \quad (3)$$

It has been usual to do these plots for fixed values of λ and also of V_{cb} or A. In our maximum likelihood approach we note that each potential value in the ρ-η plot must be considered separately for evaluating the probability of it being the correct pair of values. We thus look through all values of the CKM angles that give the same ρ and η, and find the least χ^2 in the total set to assign to the maximum likelihood for the correct answer being that pair of ρ and η. By fitting all ten experiments together, the combined χ^2 takes into account the statistical weight of the various intersection areas, instead of the usual display of the 1σ contours for each of three experiments separately, in which combined statistical weight is hard to judge by eye. We show plots for $m_t = 110$, 150, and 200 GeV corresponding to the widest range of the CERN e^+e^- collider LEP [29] for m_t of 111–197 GeV and the Collider Detector at Fermilab (CDF) and D0 lower bounds.

The maximum likelihood ρ-η plot is shown in Fig. 2(b) for $m_t = 150$ GeV. The line contours shown correspond to confidence levels associated with 1σ or 68.3% ($\chi^2 = 7.0$), 2σ or 95.4% ($\chi^2 = 12.8$), and 3σ or 99.7% ($\chi^2 = 20.1$).

The unitarity triangle has base corners on the ρ axis at $\rho = 0$ (with enclosed angle $\gamma = \delta$) and at $\rho = 1$ (with enclosed angle β), and the third corner is at the ρ-η value with enclosed angle α.

In Fig. 2(b) are also shown lines of constant values

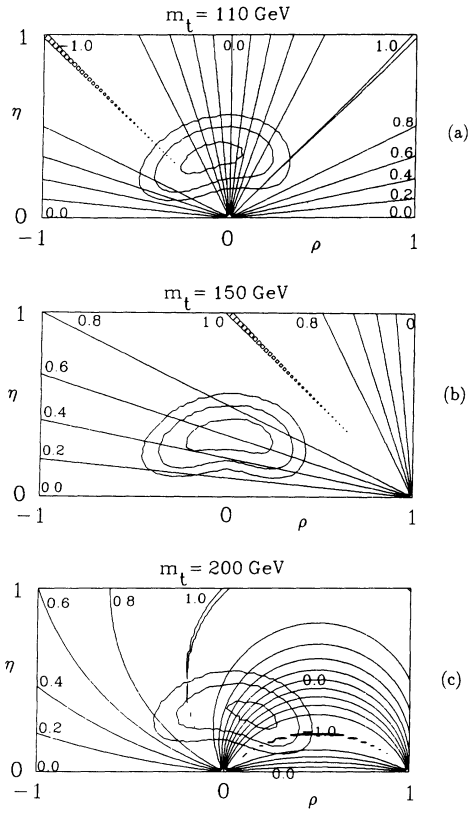

FIG. 2. Maximum likelihood ρ-η plot with the closed contours corresponding to C.L. of 1σ, 2σ, and 3σ. The straight lines show the values of the CP-violating B decay asymmetry experiments proportional to $\sin(2\gamma) = \sin(2\delta)$ in (a) for $m_t = 110$ GeV, to $\sin(2\beta)$ in (b) for $m_t = 150$ GeV, and to $\sin(2\alpha)$ in (c) for $m_t = 200$ GeV.

[27] of $\sin(2\beta)$ emanating from $\rho = 1.0$, $\eta = 0$, and separated by 0.2. The CP-violating B_d^0 decay asymmetries for $\bar{b} \to \bar{c}c\bar{s}$ such as the standard $B_d^0 \to \psi K_S$, and $\bar{b} \to \bar{c}c\bar{d}$ in $B_d^0 \to D^+D^-$, are proportional to $\sin(2\beta)$ [30]. We see that since the height of the experimental rays are proportional to $\sin(2\beta)$ rather than to $\sin\beta$ as η is, the experimental results varies roughly twice as fast for increasing β as η does, giving a factor of 2 improvement in the errors associated with determining η by measuring β. Similar comments apply to the figures below with angles $\gamma = \delta$ and α.

In Fig. 2(a) are shown the joint χ^2 contours as described above but with $m_t = 110$ GeV. Also shown are lines of constant values of results for the CP-violating B^0 decay asymmetries proportional to $\sin(2\delta) = \sin(2\gamma)$ with lines separated by 0.2. This angle shows up in quark subprocesses of $\bar{b} \to \bar{u}u\bar{d}$ in B_s decays as in $B_s \to \rho K_S$ [30].

In Fig. 2(c) are shown the likelihood contours at $m_t = 200$ GeV. The movement of the contours to higher ρ at higher m_t are due to the $K_L \to \mu\mu$ limit on short-distance second-order weak processes and the B-$\bar{B}$ mixing contours, both of which move to smaller $(1 - \rho)$ with increasing m_t. Also shown are lines of constant values of $\sin(2\alpha)$ which emanate in arcs from the origin. Inter-

vening lines are separated by 0.2. The CP-violating B_d^0 decay asymmetries proportional to these are for $\bar{b} \to \bar{u}ud$ as in $B_d^0 \to \pi^+\pi^-$.

We see in all three of these plots of superimposing the CP-violating lines, that just the value of η by itself does not determine the magnitude of the experiments, but the detailed location of the vertex in the ρ-η plane. It is also striking and important how the $\sin(2\beta)$ and $\sin(2\gamma)$ lines intersect at large crossing angles. Along with the fine grained spacing of the $\sin(2\alpha)$ contours we see how two or all three types of experiments will locate the CP-violating value of η and also ρ to a high precision.

To investigate the effect of a change in the central value of $\sqrt{B_B} f_B$, we have studied contours with this decreased by 1σ from 220 ± 40 MeV to 180 ± 40 MeV. The effect is that the right-hand side of the contours moves to the left by about $1/2\sigma$, corresponding to an increase of the $|V_{td}|$ side of the unitarity triangle by about 7%.

V. CONCLUSIONS

We have fitted ten experiments constraining the four angles in the CKM matrix, expresssing the results in terms of an overall χ^2 for each set of the four angles. We have shown by χ^2 surfaces in the three angle plots the shape in the θ_{13} and θ_{23} plane, and the changes of this cross section with variation in δ. The lower limit on θ_{23} or $|V_{cb}|$ from the joint analysis is improved over the 1σ lower limit on $|V_{cb}|$ by itself so that that value now becomes a 2σ lower bound. We have also shown how the values of the three classes of CP-violating B^0 decay asymmetries show up on the ρ-η plane and how they complement each other in providing a high resolution in this plane. Even at the 2σ level there is a signal expected from CP-violating B^0 decay asymmetries [31]. At $m_t = 150$ GeV the signal for the $\sin(2\beta)$ processes in Fig. 2(b) is at least $\sin(2\beta) \geq 0.25$ at 2σ and at 1σ the signal is at least $\sin(2\beta) \geq 0.40$, with the most probable signal at $\sin(2\beta) = 0.6 \pm 0.2$.

ACKNOWLEDGMENTS

This research was supported in part by the U.S. Department of Energy under Contract No. DE-FG03-91ER40679 and by NSF-PHY-9100825. We would also like to thank Dr. Allen Schiano and the UCI VisLab for their support. D.S. also acknowledges the Aspen Center for Physics and SLAC for their hospitality.

[1] M. Kobayashi and T. Maskawa, Prog. Theor. Phys. **49**, 652 1979).
[2] N. Cabibbo, Phys. Rev. Lett. **10**, 531 (1963).
[3] F. Gilman and Y. Nir, Annu. Rev. Nucl. Part. Sci. **40**, 213 (1990).
[4] G. Belanger and C.Q. Geng, Phys. Rev. **43**, 140 (1991).
[5] L.-L. Chau and W.-Y. Keung, Phys. Rev. Lett. **53**, 1802 (1984).
[6] N. Isgur and M.B. Wise, Phys. Lett. B **237**, 527 (1990); E. Eichten and B. Hill, *ibid.* **234**, 511 (1990); M. Neubert, *ibid.* **264**, 455 (1991).
[7] See references in the CKM matrix section of the Particle Data Group, K. Hikasa *et al.*, Phys. Rev. D **45**, S1 (1992), p. 111.65.
[8] For a critique, see S. Stone, in *B Decays*, edited by S. Stone (World Scientific, Singapore, 1992).
[9] D. Karlen, B Hadron Lifetimes, Proceedings of the Fifth International Symposium, Montreal, 1993 (unpublished).
[10] M. Artuso, in *Snowmass Workshop on B Physics at Hadron Accelerators*, AIP Conf. Proc. (AIP, New York, in press); J. Bartelt *et al.*, Phys. Rev. Lett. **71**, 4111 (1993).
[11] M. Artuso, Phys. Lett. B **311**, 307 (1993).
[12] G. Altarelli *et al.*, Nucl. Phys. **B208**, 365 (1982).
[13] J.G. Koerner and G.A. Schuler, Z. Phys. C **38**, 591 (1988).
[14] M. Wirbel, B. Stech, and M. Bauer, Z. Phys. C **38**, 511 (1988).
[15] N. Isgur, D. Scora, B. Grinstein, and M.B. Wise, Phys. Rev. D **39**, 799 (1989).
[16] A. Bean *et al.*, Phys. Rev. Lett. **70**, 2681 (1993).
[17] A. Abada *et al.*, Nucl. Phys. **B376**, 172 (1992); C.W. Bernard, J.N. Labrenz, and A. Soni, Phys. Rev. D **49**, 1589 (1994).
[18] A.J. Buras, Nucl. Phys. **B347**, 491 (1990).
[19] A.J. Buras and M.K. Harlander, in *Heavy Flavors*, edited by A.J. Buras and M. Lindner (World Scientific, Singapore, 1992).
[20] R. Gupta *et al.*, Phys. Rev. D **47**, 5113 (1993); N. Ishizuka *et al.*, Phys. Rev. Lett. **71**, 24 (1993).
[21] A.J. Schwartz, in *The Fermilab Meeting*, Proceedings of the Annual Meeting of the Division of Particles and Fields of the APS, Batavia, Illinois, 1992, edited by C. Albright *et al.* (World Scientific, Singapore, 1993). An earlier published value is in A. Heinson *et al.*, Phys. Rev. D **44**, 1 (1991).
[22] T. Akagi, Phys. Rev. Lett. **67**, 2618 (1991).
[23] Particle Data Group, G.P. Yost *et al.*, Phys. Lett. B **204**, 1 (1988).
[24] M.K. Gaillard and B.W. Lee, Phys. Rev. D **9**, 897 (1974).
[25] T. Inami and C.S. Lim, Prog. Theor. Phys. **65**, 297 (1981).
[26] M. Schmidtler and K.R. Schubert, Z. Phys. C **53**, 347 (1992).
[27] J. Rosner, in *B Decays* [8].
[28] L. Wolfenstein, Phys. Rev. Lett. **51**, 1945 (1983).
[29] S.C.C. Ting, in *The Fermilab Meeting* [21], p. 53.
[30] Y. Nir and D. Silverman, Nucl. Phys. **B345**, 301 (1990); Phys. Rev. D **42**, 1477 (1990).
[31] For a 1σ overlap region analysis, see Y. Nir and U. Sarid, Phys. Rev. D **47**, 218 (1993).

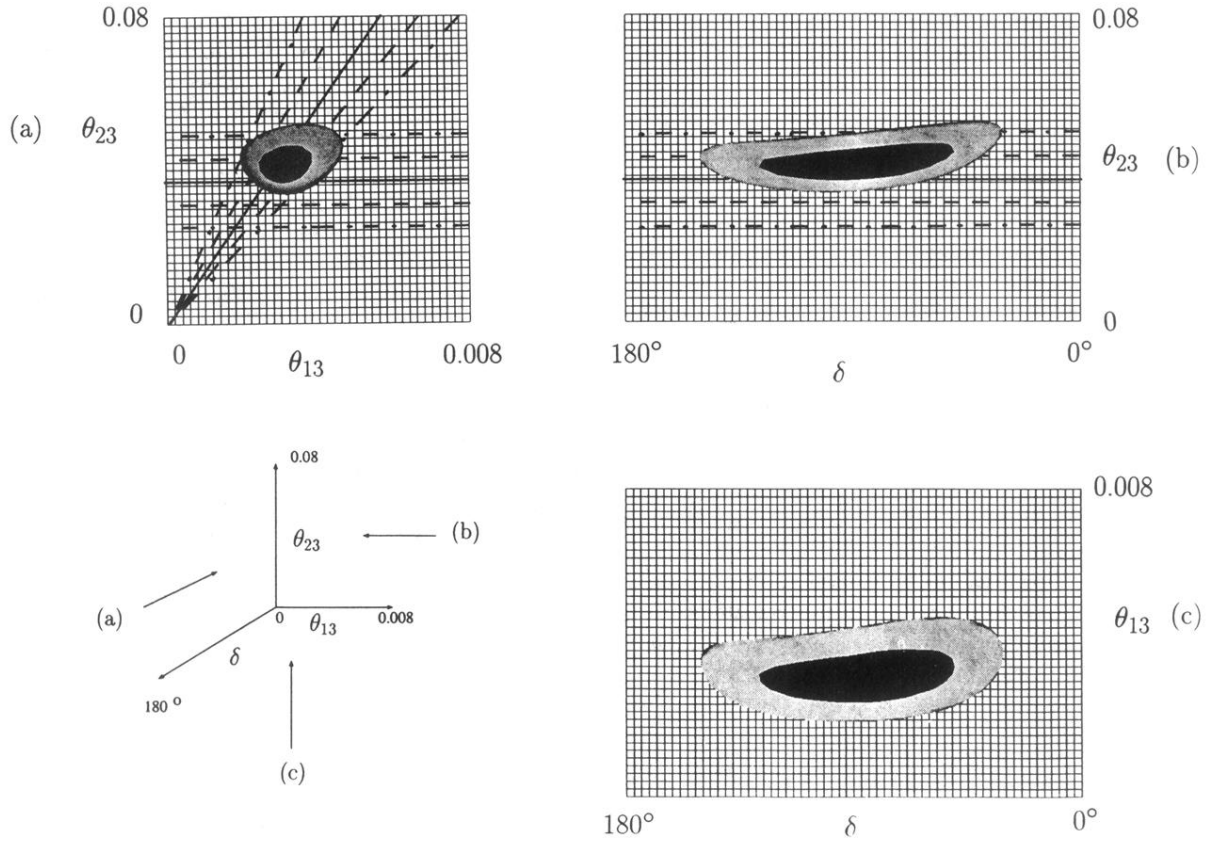

FIG. 1. Views of the three-dimensional angular plot showing the surfaces of $\chi^2 = 7.0$ and $\chi^2 = 12.8$ corresponding to 1σ and 2σ, respectively, with variables from $0 \leq \theta_{23} \leq 0.08$, $0 \leq \delta \leq 180°$, and $0 \leq \theta_{13} \leq 0.008$, for fixed $\theta_{12} = 0.223$ and $m_t = 150$ GeV. For comparison are shown in (a) and (b) central values and limits from Eqs. (1) and (2) without the maximum likelihood method. Central values are solid lines, 1σ limits are dashed lines and 2σ limits are dot-dashed lines.